Generation of nanosecond 2.65 μm pulses and pulse narrowing in fiber-bulk Ho^{3+}:YAG laser pumped gain-switched Cr^{2+}:CdSe laser

Hengkang Zhang (张恒康)[1,2,†], Encai Ji (吉恩才)[3,†], Bin Zhang (张 彬)[1,2], Yi Chen (陈 毅)[4], Baoquan Yao (姚宝权)[4], and Qiang Liu (柳 强)[1,2,*]

[1]*Key Laboratory of Photonic Control Technology (Tsinghua University), Ministry of Education, Beijing 100084, China*
[2]*State Key Laboratory of Precision Measurement Technology and Instruments, Department of Precision Instrument, Tsinghua University, Beijing 100084, China*
[3]*School of Electronic and Information Engineering, Harbin Institute of Technology, Shenzhen 518055, China*
[4]*National Key Laboratory of Tunable Laser Technology, Harbin Institute of Technology, Harbin 150001, China*
**Corresponding author: qiangliu@mail.tsinghua.edu.cn*

Received October 31, 2019; accepted December 11, 2019; posted online March 9, 2020

The generation of mid-infrared pulsed lasers was achieved in a Ho^{3+}:YAG laser pumped gain-switched Cr^{2+}:CdSe laser system with the shortest pulse duration of 4.15 ns. With a pump pulse duration of 50 ns and pump power of 2.7 W, the gain-switched Cr^{2+}:CdSe laser achieved over 10 times pulse narrowing, obtaining the maximum peak power of 5.7 kW. The optical-to-optical conversion efficiency was 3.7%, which could be further improved with better crystal surface polishing quality. The laser central wavelength was measured to be 2.65 μm with a bandwidth (FWHM) of 50 nm. In addition, the parameter optimization for suppressing the pulse tail was discussed, while the long cavity and high output transmissivity contributed to obtaining the single-peak pulses.

Keywords: Cr^{2+}:CdSe laser; gain-switching; pulse narrowing; mid-infrared.
doi: 10.3788/COL202018.031403.

The mid-infrared spectral range is known as the "molecular fingerprint" region. Particularly, the 2–3 μm section overlaps the fundamental vibrational absorption lines of water vapor, carbon dioxide, and the other gases[1–3]. Broad-emission-bandwidth lasers operating in this region have great significance in numerous applications, such as attosecond transient absorption spectroscopy, atmospheric remote sensing, frequency metrology, laser surgery, and industrial processing[4–9]. Nonlinear optical technologies, including optical parametric oscillators and difference frequency generators, are normally employed to generate mid-infrared lasers due to their wide wavelength tunability, but they suffer from a lack of robustness and compactness. Sustained effort has been expended to find solid-state laser materials for direct mid-infrared light generation. In 1996, DeLoach *et al.,* from Lawrence Livermore Laboratory, demonstrated the spectroscopic characteristics of divalent transition metal ions doped II-VI semiconductors and indicated the advantages of Cr^{2+}-doped chalcogenide crystals as a novel class of tunable mid-infrared gain media for their broad and smooth emission band located in the 2–3 μm region[10]. Then interest was inspired in the research of this class of materials, and laser oscillations of Cr^{2+}-doped ZnSe, ZnS, CdSe, CdMnTe, etc., were gradually realized[11–13]. Among the materials, Cr^{2+}:CdSe attracted plenty of attention for its large emission cross section and ultra-broad emission band (2.2–3.6 μm)[14,15].

After McKay *et al.*[16,17] reported the broadly tunable laser oscillation of Cr^{2+}:CdSe, a series of subsequent research on the gain-switched Cr^{2+}:CdSe laser was demonstrated, while pulsed Tm^{3+} or Ho^{3+} lasers were usually employed as a pump source[18,19]. In 2018, an x-fold Cr^{2+}:CdSe resonator pumped by a nanosecond Tm:YAP laser was reported by Martynova *et al.*[20], with the average output power of 420 mW and a pulse duration of 200 ns. In the same year, Yumoto *et al.*[21] reported the output energy scaling of a Cr^{2+}:CdSe laser pumped by a high-energy 420 ns Tm:YAG laser, producing a maximum output energy of 4.4 mJ at 2.64 μm. They also presented the multi-peak temporal profile of the output pulse, and the duration of the primary spike pulse was 32 ns. In 2019, Antipov *et al.* reported the highest output power of a 6.3 W gain-switched Cr^{2+}:CdSe laser with a pulse duration of about 50 ns[22]. These works have shown a good performance of Cr^{2+}:CdSe for pulsed operation, but the laser pulse durations in most of the above works are more than dozens of nanoseconds. A narrow laser pulse that is shorter than 10 ns has been achieved in the recent research[22]; however, there has not been any detailed discussion about the generation method and its parameter optimization. Since the mid-infrared narrow pulses are crucial for the applications with time resolution requirements, in 2015, Mirov *et al.* reported the narrow-pulse laser in the gain-switched regime with Cr^{2+}:ZnSe and Cr^{2+}:ZnS as the gain medium, and the pulse duration was in the 3.3–5.3 ns range depending on the repetition rate[23]. It is also worth achieving the narrow-pulse operation of a Cr^{2+}:CdSe laser, as Cr^{2+}:CdSe has a longer peak-emission-wavelength and a broader wavelength tuning range than Cr^{2+}:ZnSe/ZnS.

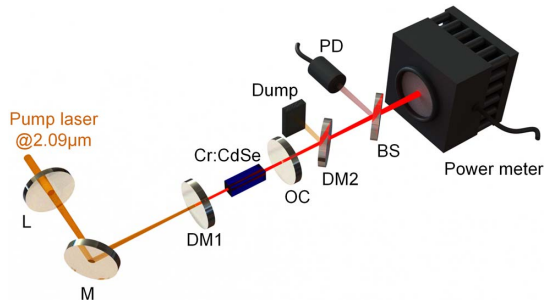

Fig. 1. Schematic diagram of the gain-switched Cr^{2+}:CdSe laser. L: plano-convex lens; DM: dichroic mirror; OC: output coupler; BS: beam splitter; PD: photodetector.

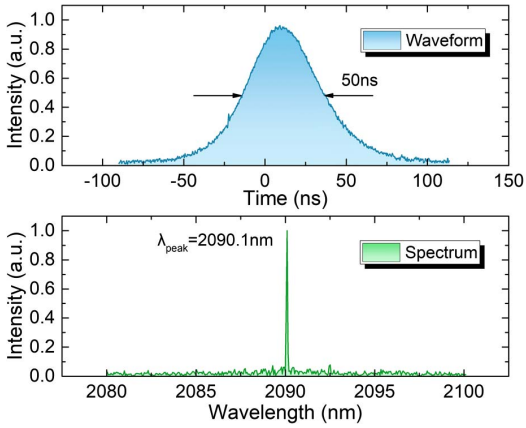

Fig. 2. Pump laser pulse profile and spectrum.

In our previous work, a quality Cr^{2+}:CdSe crystal was analyzed and applied as a saturable absorber in a Ho^{3+}:YAG Q-switched laser system[24]. In this Letter we attempted to study the pulse narrowing phenomenon in the Cr^{2+}:CdSe laser pumped by 50 ns holmium laser pulses and verify its feasibility for generating a several-nanosecond-level mid-infrared laser. After that, we discussed the parameter optimization for obtaining single-peak output pulses.

In the schematic diagram of the gain-switched Cr^{2+}:CdSe laser shown in Fig. 1, a linear cavity consisting of a plane dichroic mirror [DM1, antireflection (AR)-coated from 1.9 to 2.1 μm and high reflection (HR)-coated from 2.5 to 2.9 μm] and a plane output coupler (OC, AR-coated from 1.9 to 2.1 μm, reflectivity $R = 80\%$ from 2.5 to 2.9 μm) was employed, and the cavity geometrical length was 45 mm. The 16 mm long Cr^{2+}:CdSe crystal was grown by the vertical Bridgman method at a high speed, which sacrifices the crystalline structure. The doping concentration of Cr^{2+} is $1.0 \times 10^{18}\,\mathrm{cm}^{-3}$. Both the end faces were AR-coated at 1.9–2.1 μm and 2.5–2.9 μm, and the crystal was placed 15 mm away from DM1. The intrinsic loss of the crystal should be relatively large, due to its imperfect crystalline structure and polishing quality. The crystal was wrapped with indium foil and was mounted on a copper heat sink, then kept at a constant temperature of 14°C by using a thermoelectric cooler (TEC). The laser cavity was designed with the consideration of stability conditions, while the thermal lens effect of the crystal was estimated by the expression[25]

$$f_T = \frac{2\pi K_c}{\mathrm{d}n/\mathrm{d}T + \alpha_T n} \times \frac{\omega_{\mathrm{eff}}^2}{\eta_Q \eta_a P_{\mathrm{in}}}, \tag{1}$$

where f_T represents the thermal focal length, $K_c = 9\,\mathrm{W \cdot K^{-1} \cdot m^{-1}}$ is the thermal conductivity of the crystal, $\mathrm{d}n/\mathrm{d}T = 1 \times 10^{-4}\,\mathrm{K}^{-1}$ is the thermo-optical coefficient, $\alpha_T = 6.3 \times 10^{-6}\,\mathrm{K}^{-1}$ is the coefficient of thermal expansion[26], n is the refractive index, ω_{eff} is the effective pump radius, η_Q is the quantum efficiency, η_a is the absorption efficiency, and P_{in} is the incident pump power.

A Tm:fiber-laser-pumped Q-switched Ho^{3+}:YAG laser operating at a pulse repetition frequency (PRF) of 1 kHz with a maximum output power of 2.7 W worked as the pump source. The pump pulse profile and spectrum are shown in Fig. 2 with a pulse duration (FWHM) of about 50 ns and a central wavelength of 2090.1 nm. The pump laser was focused into the crystal by an AR-coated plano-convex lens (L) with a focal length of 100 mm. The estimated focal spot radius was about 250 μm, resulting in a maximum pump density of nearly $1.4\,\mathrm{J/cm^2}$, which was lower than the damage threshold of the film (about $2.5\,\mathrm{J/cm^2}$). The unabsorbed pump laser was removed by the dichroic mirror (DM2) after the OC. Then the beam splitter (BS), with a reflectivity of 1%, sampled the output laser, and the HgCdTe photodetector (VIGO System S.A. PVM-10.6) measured the pulse profile. The output power was measured by a power meter (Ophir, 30A-BB-18), while the output spectrum was measured by a monochromator (BOIF, WDM1-3). By substituting the related parameters into Eq. (1), we found that the thermal focal length of the crystal at 2.7 W pump power was about 68.9 mm. It was verified that the cavity remained stable when the pump power varied from zero to 2.7 W.

The output power of the gain-switched Cr^{2+}:CdSe laser is shown in Fig. 3, and optical damage was not observed on the surfaces of the crystal. The output power increased linearly with the pump power, then reached a maximum value of 100 mW with a pump power of 2.7 W. The optical-to-optical conversion efficiency was only 3.7%, which resulted from the imperfect crystalline structure and the low polished quality. Without the cavity, we measured that the transmissivity of the crystal to the pump laser was about 18%. It was given that the absorptivity of the crystal was about 77.8%, and we estimated that the intrinsic loss coefficient was about $0.13\,\mathrm{cm}^{-1}$. We assumed that the loss coefficient at the pump wavelength was the same as that at the signal wavelength; therefore, the signal laser would suffer an intrinsic loss of 34% in a round trip. The inset (a) in Fig. 3 exhibits the normalized temporal profile of the output pulse versus the pump pulse under the maximum pump condition. The profile of the output pulse was featured by multiple peaks, which was

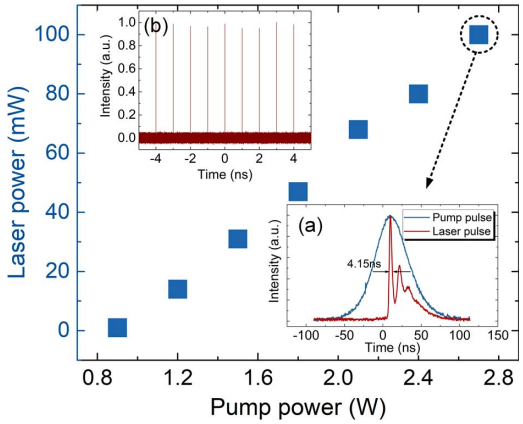

Fig. 3. Power performance of the gain-switched Cr^{2+}:CdSe laser. Inset (a): the temporal profiles of the Cr^{2+}:CdSe laser and the Ho^{3+}:YAG laser under the maximum pump power. Inset (b): the pulse train under the maximum pump power.

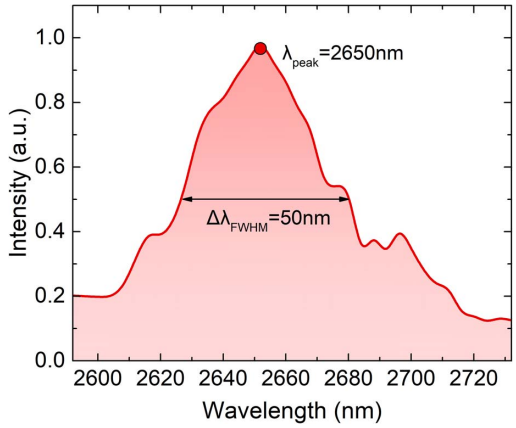

Fig. 4. Output spectrum of the Cr^{2+}:CdSe laser.

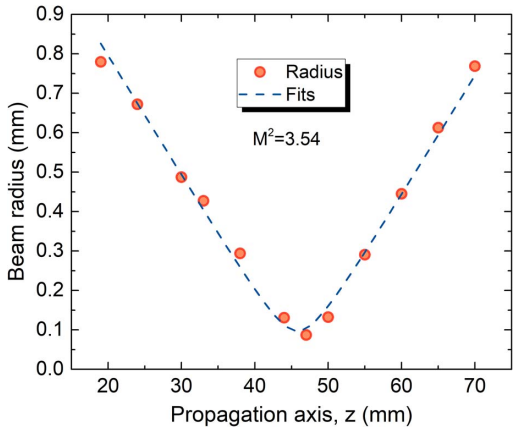

Fig. 5. Beam quality of the Cr^{2+}:CdSe laser.

mentioned by many of the literatures about gain-switched lasers[23,27,28]. Owing to the high pump rate of the nanosecond pump pulse, the medium could achieve a high optical gain that was far above the threshold. Therefore, the signal laser intensity could increase rapidly and form a spike pulse that is narrower than the pump pulse. Then, with the injection of the subsequent part of the pump pulse, the relaxation oscillation process modulated the profile of the signal pulse, resulting in the formation of a multi-peak tail. For gain-switched laser operation, the output pulse is normally characterized by the pulse duration and the peak power of the primary spike pulse[23,27]. In our experiment, the duration of the spike pulse was only 4.15 ns, which was below one-tenth of the pump duration. This result indicated that over 10 times pulse narrowing could be realized in the Cr^{2+}:CdSe laser; therefore, we can obtain several-nanosecond-level pulses with much broader pump pulses. The inset (b) in Fig. 3 depicts the pulse sequence under the maximum pump power. The standard deviation of the pulse peak intensity was used to describe the pulse stability, and it was calculated as 1.85% here. The spectrum of the Cr^{2+}:CdSe laser is depicted in Fig. 4; the peak wavelength was 2.65 μm and the bandwidth (FWHM) was about 50 nm without a wavelength-selection element. The beam quality of the laser was measured with the knife-edge method, and the result is shown in Fig. 5, where the M^2 factor was 3.54. This relatively high M^2 factor was due to the employment of the short cavity. The imperfect crystalline structure and the low polished quality would also hinder the improvement of the beam quality.

The temporal profiles of output pulses under different pump powers, with a step of 0.3 W, are shown in Fig. 6(a). Meanwhile, based on the laser properties of the Cr^{2+}:CdSe crystal, we built a theoretical model and conducted a numerical investigation of the pulses profiles. The validity of the model was verified by comparing the theoretical and experimental results, and then the model helped to perform the parameter optimization of the laser.

Free Cr^{2+} ions with $3d^4$ configuration have a ground state of ^5D. When Cr^{2+} ions are doped into the chalcogenide crystals, the tetrahedral crystal field will split the ^5D state into triplet $^5T_2$ and duplet ^5E. Transitions between the two states are the main kinetic processes relating to the mid-infrared laser operation of Cr^{2+}-doped chalcogenide crystals, since the other transitions from the ground state $^5T_2$ or the excited state ^5E to upper lying states are spin forbidden[14,29]. The Jahn–Teller effect causes further splitting of the states[30,31], making the states no longer a line energy level but a broad energy band. Therefore, Cr^{2+}-doped chalcogenide crystals have an ultra-broad absorption and emission band.

The studies of laser dynamics showed that the two-energy-band structure in Cr^{2+}-doped chalcogenide crystals has similar transition properties to four-level systems because the in-band nonradiative decay exists in both bands. The four-level rate equations have been applied in the theoretical investigation of the Cr^{2+}:ZnSe laser[32]. Although the single frequency does not conform to the situation of the wide-bandwidth laser, it provides an approximation for the laser oscillation since all the frequency components have nearly the same gain. Here we also utilize a four-level system to model the energy level

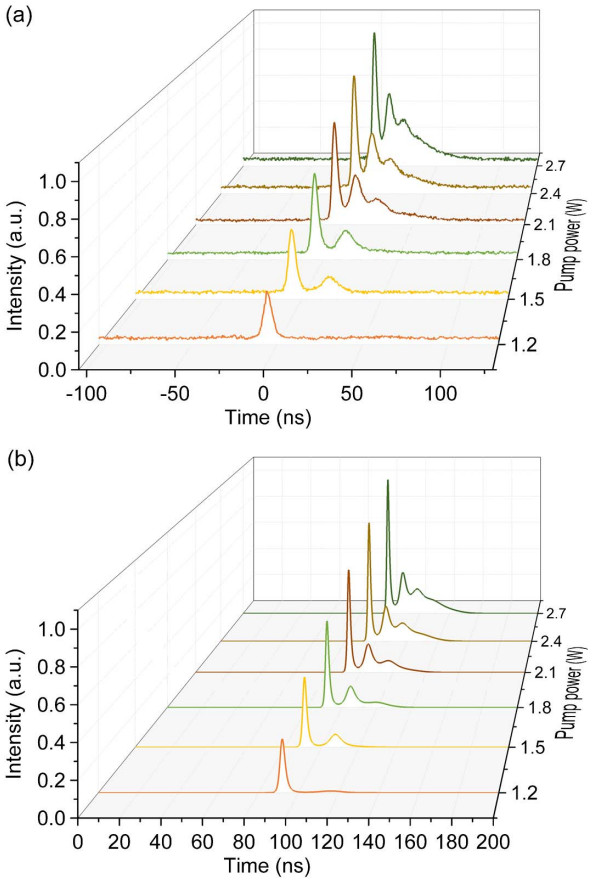

Fig. 6. Temporal profiles of the output pulses under different pump powers: (a) experimental results; (b) simulation results.

structure of Cr^{2+}:CdSe. By neglecting the spatial distribution, the rate equations of the population inversion density and photon density can be expressed as[28]

$$\frac{\mathrm{d}\Delta N(t)}{\mathrm{d}t} = R_p(t) - c\sigma_e\Phi(t)\Delta N(t) - c\sigma_{\mathrm{esa}}\Phi(t)\Delta N(t) - \frac{\Delta N(t)}{\tau}, \tag{2}$$

$$\frac{\mathrm{d}\Phi(t)}{\mathrm{d}t} = c\sigma_e\Phi(t)\Delta N(t)\frac{L_0}{L} - c\sigma_{\mathrm{esa}}\Phi(t)\Delta N(t)\frac{L_0}{L} - \frac{\Phi(t)}{\tau_c}. \tag{3}$$

$\Delta N(t)$ and $\Phi(t)$ represent the population inversion density and photon density, respectively. σ_e is the emission cross section of Cr^{2+}:CdSe, and σ_{esa} is the absorption cross section of the excited level at the lasing wavelength. The excited-state absorption is negligible because the transition is spin-forbidden and σ_{esa} is much smaller than σ_e. This has been confirmed by the study of Cr^{2+}:ZnSe, which works as the gain medium and saturable absorber[32,33]. c is the velocity of light in vacuum, $R_p(t)$ is the pump rate, τ is the fluorescence lifetime of the excited state, and τ_c is the photon lifetime of the cavity. L_0 and L represent the length of the Cr^{2+}:CdSe crystal and the cavity, respectively. For the gain-switched operation pumped by Gaussian nanosecond pulses, the pump rate can be expressed as

$$R_p(t) = \frac{P_{\mathrm{peak}}\eta_a}{Vh\nu_p}\exp\left(-\frac{4\ln 2\times t}{t_p}\right)^2, \tag{4}$$

where P_{peak} is the peak pump power, t_p is the pump pulse duration, V is the gain volume, h is the Planck constant, ν_p is the pump laser frequency, and η_a is the pump absorption efficiency, which is defined as

$$\eta_a = 1 - \exp\{-\sigma_a[N_0 - \Delta N(t)]L_0\}, \tag{5}$$

where σ_a is the absorption cross section of Cr^{2+}:CdSe and N_0 is the Cr^{2+} doping concentration.

The parameters listed in Table 1 were used to conduct the numerical simulation. The values of the parameters come from Refs. [15,26,34]. The pump duration and pump power were the same as that in the experiment. The simulation results are shown in Fig. 6(b). It can be found that compatible results are obtained from the experiment and simulation. The narrow spike pulse could be always observed at the rising edge of the pulse profile, whereas the shape and intensity of the pulse tail varied with the pump power. At a low pump power of 1.2 W, the pulse had a single-peak profile. As the pump power increased, the pulse build-up time of the signal pulse decreased, and the location of the spike pulse moved forward. More pump power was converted into the pulse tail, which formed after the primary spike pulse, leading to a gradual increase in the intensity.

The pulse duration of the spike pulse was measured in the experiment and is depicted in Fig. 7(a) by triangle dots. The minimum pulse duration of 4.15 ns was achieved at the maximum pump power. The simulation results of the spike pulse duration are illustrated by the solid line, which have the same tendencies as the experimental results. Nevertheless, the calculated values were lower than

Table 1. Parameters Used in the Numerical Simulation

Parameter	Value[15,26,34]
Refractive index at 2.65 μm, n	2.46
Absorption cross section at 2.09 μm, σ_a	1.94×10^{-18} cm^2
Emission cross section at 2.65 μm, σ_e	2.0×10^{-18} cm^2
Fluorescence lifetime at 287 K, τ	3.7 μs
Crystal length, L_0	16 mm
Cavity length, L	45 mm
Doping concentration of Cr^{2+}, N_0	1.0×10^{18} cm^{-3}
Transmissivity of OC, T_{OC}	20%
Intrinsic loss coefficient, α	0.13 cm^{-1}

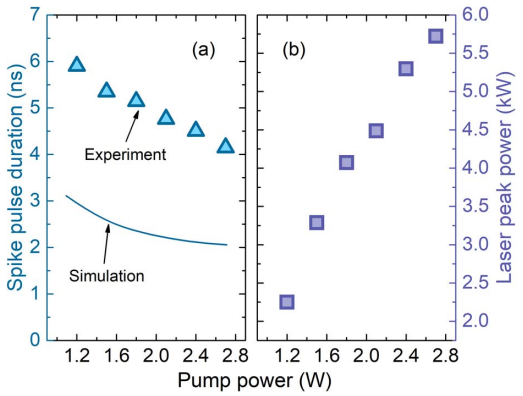

Fig. 7. (a) Pulse duration and (b) peak power of the output pulse under different pump powers.

the measured values, which we determined for the following two reasons. One was the calculation error induced by neglecting the spatial distribution of the laser beam, and the other one was that we simplified the broadband signal laser as monochromatic light. Based on the pulse energy and the temporal profile measured in the experiment, the peak power of the spike pulse was calculated by using the expression

$$P_{\text{peak}} = \frac{E_{\text{single}}}{\int_{-\infty}^{\infty} W^{\text{norm}}(t)\mathrm{d}t}, \tag{6}$$

where E_{single} is the single-pulse energy and $W^{\text{norm}}(t)$ is the normalized profile of the output pulse. The results are shown in Fig. 7(b), where the maximum peak power of 5.7 kW was obtained at the pump power of 2.7 W.

Even though we have obtained several-nanosecond-level pulses in the experiment, a practical problem is that the pulse tail always exists, and the intensity of the tail increases with the increase of the pump power. However, in the applications of the mid-infrared laser, the pulse tail would act as the noise, and hence the cavity should be optimized to obtain the single-peak output pulses. The high intrinsic loss of the crystal hinders the experimental optimization, and here we used a better-quality crystal to conduct a numerical simulation to discuss the appropriate parameter for producing the single-peak pulses.

The core idea of suppressing the pulse tail in the gain-switched laser is to control the build-up time to let the signal pulse form at the falling edge of the pump pulse[28]; therefore, the signal pulse tail is not able to extract enough gain and is suppressed. The main factors that determine the pulse build-up time include the gain and loss of the cavity and the cavity length. We fixed the pump power at 2.7 W and assumed that the intrinsic loss coefficient was 0.01 cm^{-1}; as a result, the output loss became the dominant loss term. We set up four different combinations of the cavity length and the output transmissivity. By substituting the parameters into the theoretical model, we calculated the temporal profiles of the output pulses.

For combination 1, the output transmissivity was 20%, and the cavity length was 45 mm, which was the same as that of the above experiment. The normalized temporal profiles of the signal and pump pulse are shown in Fig. 8(a). It could be found that the signal pulse formed at the rising edge of the pump pulse. The primary spike pulses had a duration of 3.14 ns, and were followed by an intense tail with a nearly-Gaussian shape. In addition, the average output power was 509.7 mW. For combination 2, the output transmissivity was 80%, and the cavity length was 45 mm. The simulation result is shown in Fig. 8(b), where the signal pulse had a multi-peak profile, the duration of the primary spike pulse was 1.24 ns, and the average output power was 397.8 mW. With these two conditions, although the output transmissivity has an obvious influence on the pulse profile, the pulse tail is still not suppressed.

For combination 3, the cavity length was enlarged to 500 mm with the output transmissivity of 20%, and the result is shown in Fig. 8(c). The signal pulse with a duration of 40.52 ns formed at the falling edge of the pump pulse. The profile had a single peak, but the pulse duration was relatively large, while the average output power was 323.1 mW. Figure 8(d) shows the result of combination 4; the output transmissivity was 80% and the cavity length was 500 mm. A single-peak signal pulse with a duration of only 8.17 ns formed at the falling edge of the pump pulse, and the average output power was 117.2 mW. From these results we know that the signal pulse tail could be suppressed by employing a long cavity, as large cavity length corresponds to long pulse build-up time. Then high output transmissivity could help to reduce the pulse duration; therefore, the several-nanosecond-level single-peak pulses could be obtained at the cost of output power.

In conclusion, for a fiber-bulk Ho^{3+}:YAG laser pumped gain-switched Cr^{2+}:CdSe laser, the generation of high-peak-power nanosecond mid-infrared pulses was demonstrated, and the experimental results highly agreed with the simulation. Under 2.7 W pump power, a pulse duration of 4.15 ns, which was shorter than one-tenth of the pump duration was obtained. To the best of our knowledge, this is the shortest pulse duration ever reported for a Cr^{2+}:CdSe laser, which shows that the gain-switched Cr^{2+}:CdSe laser could achieve over 10 times pulse narrowing, while the corresponding peak power was 5.7 kW. The optical-to-optical conversion efficiency was 3.7%, which should be further improved with better crystal surface polishing quality. The laser central wavelength was 2.65 μm with a bandwidth (FWHM) of 50 nm. Meanwhile, the parameter optimization for generating single-peak pulses was discussed by numerical simulations. When a 500 mm long cavity and 80% output transmissivity were employed, the tail of the output pulses could be suppressed and 8.77 ns single-peak pulses could be obtained with a better-quality crystal. Our demonstration has great significance for the time-resolution applications of mid-infrared lasers, and future efforts will be spent on the

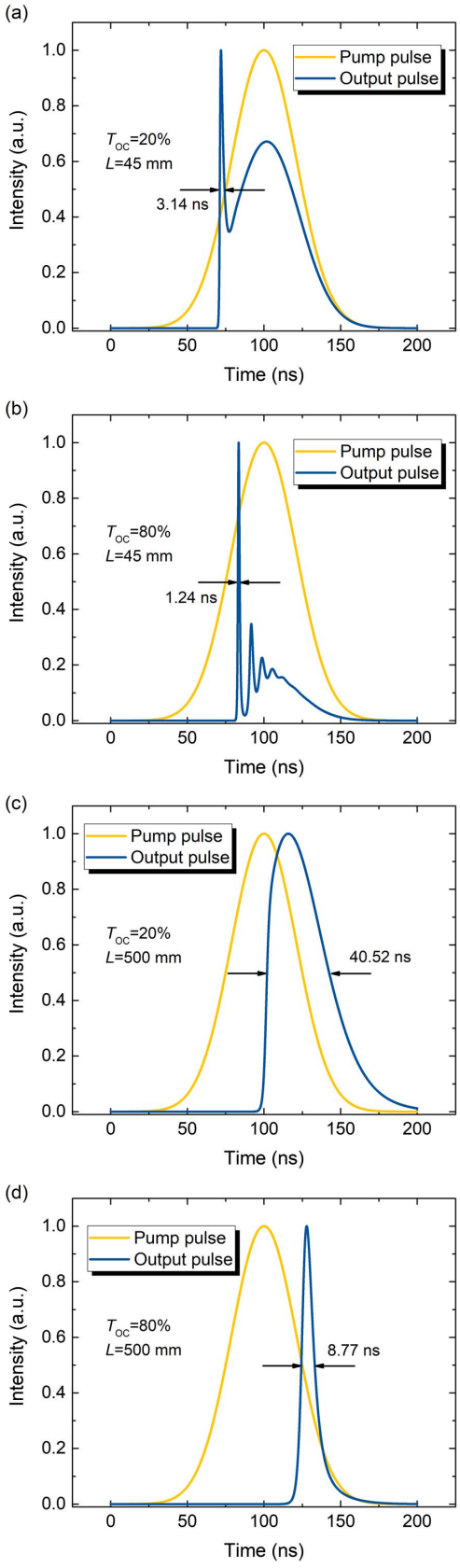

Fig. 8. Temporal profiles of the output pulse and the pump pulse with (a) 20% output transmissivity, 45 mm cavity length; (b) 80% output transmissivity, 45 mm cavity length; (c) 20% output transmissivity, 500 mm cavity length; (d) 80% output transmissivity, 500 mm cavity length.

further optimization of the crystal quality, the Cr^{2+} doping concentration, the output transmissivity, and the cavity length to suppress the tail of the output pulse and to improve the conversion efficiency.

This work was supported by the National Key Research and Development Program of China (No. 2017YFB1104500), the China Postdoctoral Science Foundation (No. 2018M630355), and the National Natural Science Foundation of China (Nos. 61905128 and 61905150).

†These authors contributed equally to this work.

References

1. I. T. Sorokina, in *Mid-Infrared Coherent Sources and Applications*, M. Ebrahim-Zadeh and I. T. Sorokina, eds. (Springer, 2008), p. 225.
2. S. B. Mirov, V. V. Fedorov, D. V. Martyshkin, I. S. Moskalev, M. S. Mirov, and V. P. Gapontsev, Opt. Mater. Express **1**, 898 (2011).
3. X. Guo, Q. Wu, L. Guo, F. Ma, F. Tang, C. Zhang, J. Liu, B. Mei, and L. Su, Chin. Opt. Lett. **16**, 051401 (2018).
4. S. B. Mirov, V. V. Fedorov, I. S. Moskalev, and D. V. Martyshkin, IEEE J. Sel. Top. Quantum Electron. **13**, 810 (2007).
5. T. Lin, A. Aoki, N. Saito, M. Yumoto, S. Nakajima, K. Nagasaka, S. Ichinose, K. Mizutani, S. Wada, and Y. Izumi, Lasers Surg. Med. **48**, 965 (2016).
6. L. Maidment, Z. Zhang, C. R. Howle, and D. T. Reid, Opt. Lett. **41**, 2266 (2016).
7. G. Ycas, F. R. Giorgetta, E. Baumann, I. Coddington, D. Herman, S. A. Diddams, and N. R. Newbury, Nat. Photonics **12**, 202 (2018).
8. J. Xue, C. Liu, Z. Zeng, R. Li, and Z. Xu, Chin. Opt. Lett. **17**, 082601 (2019).
9. J. Wu, Y. Ju, B. Yao, T. Dai, Z. Zhang, X. Duan, and Y. Wang, Chin. Opt. Lett. **15**, 031402 (2017).
10. L. D. DeLoach, R. H. Page, G. D. Wilke, S. A. Payne, and W. F. Krupke, IEEE J. Quantum Electron. **32**, 885 (1996).
11. R. H. Page, K. I. Schaffers, L. D. Deloach, G. D. Wilke, F. D. Patel, J. B. Tassano, Jr, S. A. Payne, W. F. Krupke, K. T. Chen, and A. Burger, IEEE J. Quantum Electron. **33**, 609 (1997).
12. K. L. Schepler, S. Kück, and L. Shiozawa, J. Lumin. **72**, 116 (1997).
13. J. T. Seo, U. Hömmerich, S. B. Trivedi, R. J. Chen, and S. Kutcher, Opt. Commun. **153**, 267 (1998).
14. S. Mirov, V. Fedorov, I. Moskalev, D. Martyshkin, and C. Kim, Laser Photonics Rev. **4**, 21 (2010).
15. T. T. Fernandez, M. K. Tarabrin, Y. Wang, V. A. Lazarev, S. O. Leonov, V. E. Karasik, Y. V. Korostelin, M. P. Frolov, Y. P. Podmarkov, Y. K. Skasyrsky, V. I. Kozlovsky, C. Svelto, P. Maddaloni, N. Coluccelli, P. Laporta, and G. Galzerano, Opt. Mater. Express **7**, 3815 (2017).
16. J. McKay, K. L. Schepler, and G. C. Catella, Opt. Lett. **24**, 1575 (1999).
17. G. Catella, J. Mckay, and K. L. Schepler, in *Advanced Solid State Lasers* (1999), paper WD1.
18. V. A. Akimov, V. I. Kozlovskii, V. K. Yu, A. I. Landman, P. P. K. Yu, Y. K. Skasyrskii, and M. P. Frolov, Quantum Electron. **38**, 205 (2008).
19. O. L. Antipov, I. D. Eranov, M. P. Frolov, Y. V. Korostelin, V. I. Kozlovsky, A. A. Novikov, Y. P. Podmar'kov, and Y. K. Skasyrsky, Laser Phys. Lett. **12**, 045801 (2015).
20. O. V. Martynova, S. V. Kurashkin, A. P. Savikin, and A. P. Zinoviev, Laser Phys. Lett. **15**, 065001 (2018).
21. M. Yumoto, N. Saito, T. Lin, R. Kawamura, A. Aoki, Y. Izumi, and S. Wada, Biomed. Opt. Express **9**, 5645 (2018).

22. O. L. Antipov, I. D. Eranov, M. P. Frolov, Y. V. Korostelin, V. I. Kozlovsky, and Y. K. Skasyrsky, Opt. Lett. **44**, 1285 (2019).
23. S. B. Mirov, V. V. Fedorov, D. Martyshkin, I. S. Moskalev, M. Mirov, and S. Vasilyev, IEEE J. Sel. Top. Quantum Electron. **21**, 292 (2015).
24. E. Ji, M. Nie, X. Fu, Z. Guan, and Q. Liu, Opt. Lett. **42**, 2555 (2017).
25. J. Z. Zheng, S. Z. Zhao, Q. P. Wang, X. Y. Zhang, and L. Chen, Acta Photon. Sin. **30**, 724 (2001).
26. I. T. Sorokina, in *NATO Science for Peace and Security Series B: Physics and Biophysics* (2008), p. 225.
27. J. J. Zayhowski, J. Ochoa, and A. Mooradian, Opt. Lett. **14**, 1318 (1989).
28. W. Koechner, *Solid-State Laser Engineering* (Springer, 2013), Vol. **1**.
29. M. Kaminska, J. M. Baranowski, S. M. Uba, and J. T. Vallin, J. Phys. C **12**, 2197 (1979).
30. S. I. Klokishner, B. S. Tsukerblat, O. S. Reu, A. V. Palii, and S. M. Ostrovsky, Opt. Mater. **27**, 1445 (2005).
31. D. Colignon, E. Kartheuser, S. Rodriguez, and M. Villeret, J. Cryst. Growth **159**, 875 (1996).
32. A. Sennaroglu, A. O. Konca, and C. R. Pollock, IEEE J. Quantum Electron. **36**, 1199 (2000).
33. H. Cankaya, U. Demirbas, A. K. Erdamar, and A. Sennaroglu, J. Opt. Soc. Am. B **25**, 794 (2008).
34. J.-O. Ndap, C. I. Rablau, K. Morrow, O. O. Adetunji, V. A. Johnson, K. Chattopadhyay, R. H. Page, and A. Burger, J. Electron. Mater. **31**, 802 (2002).